

# Valley polarization dynamics of monolayer $\text{WSe}_2$ measured by time-resolved PL in an attoDRY700

G. Wang, L. Bouet, D. Lagarde, M. Vidal, A. Balocchi, T. Amand, X. Marie, and B. Urbaszek  
Université de Toulouse, INSA-CNRS-UPS, LPCNO, Toulouse, France

## Introduction

The transition metal dichalcogenide (TMDC) monolayers (MLs) have been extensively studied in recent years because of their unique electronic and optical properties. The band structures of these TMDC materials undergo a crossover from indirect to direct gap semiconductors in the visible region when thinned to one ML, with potential applications in e.g. electronics as transistors or optoelectronics as LEDs [1]. An important feature of these TMDCs is that the band edge is located at the  $K$ -valleys of the hexagonal Brillouin zone. In TMDC MLs the crystal inversion symmetry breaking (see Fig. 1(a)) and the strong spin-orbit interaction result in the unique coupling of carrier spin and the  $K$ -valley index in momentum space. Therefore two types of nonequivalent  $K+$  and  $K-$  valleys are associated with  $\sigma+$  and  $\sigma-$  circularly polarized light in the interband transition process. This allows to address individual valley carriers, so called valley polarization, by circularly polarized optical excitation as shown in Figure 1(c), which makes TMDC MLs an especially promising candidate for studies on the emerging field “valleytronics”.

It is essential to examine the stability of the created valley polarization for the implementation of valleytronics applications. The optically generated initial valley polarization is expected to be stable, as the large spin-orbit interaction will suppress the valley-spin relaxation. However, strong Coulomb interactions between charge carriers, excitonic effects, dominate the optical properties in these systems with ideal 2D confinement of TMDC and lead to very intricate valley dynamics.

Our target is to investigate the stability of the valley polarization experimentally. Two different cases need to be investigated: First, the neutral exciton ( $X^0$ ), a Coulomb bound electron-hole pair, for which strong Coulomb exchange effects are expected to lead to a fast loss of valley polarization [2]. Second, the charged exciton, an  $X^0$  with an additional electron forming a trion. This state is expected to have a more robust valley polarization.

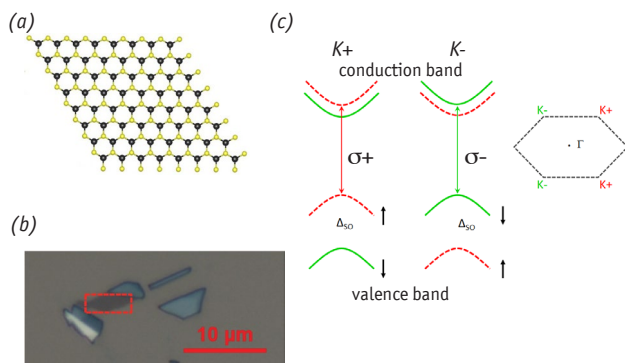


**Figure 1:** (a) Schematic of TMDC MLs structures with inversion symmetry breaking. Transition metal atoms are shown in black, chalcogen atoms in yellow [1]. (b) ML  $\text{WSe}_2$  samples are identified by optical contrast. The flake used for this note is marked with a red box. (c) Valley-contrast optical selection rules under circularly polarized laser excitation in ML  $\text{WSe}_2$ .

In the well-explored ML  $\text{MoS}_2$ , spectrally broad transitions make the distinction between the valley dynamics of the  $X^0$  and the trion currently very difficult. In this application note we employed time-resolved photoluminescence (TRPL) in another very promising material, namely monolayer  $\text{WSe}_2$ . In this 2D semiconductor with strong light-matter interaction, the  $X^0$  and trion are spectrally well-separated. Thanks to the high sample quality and the stability of our set-up, we were able to reveal for the first time a striking difference between  $X^0$  and trion valley dynamics [3]. The stable valley polarization of the trion lasting over nano-seconds makes this complex an excellent candidate for the valley Hall research and valleytronics devices.

High quality TMDC MLs samples can be obtained through mechanical exfoliation from bulk materials. The sample we used in this application note is shown in Figure 1(b). The ML flake is identified by its optical contrast and further confirmed by strong PL emission, as flakes with thicknesses  $>1$  ML are inefficient emitters due to their indirect band-gap. The typical diameter of exfoliated TMDC ML samples is around  $10 \mu\text{m}$ , therefore micro-PL and an accurate positioners with at least sub  $\mu\text{m}$  resolution are needed to locate the sample and perform optical measurements. Based on the attoDRY700 and the ANP positioners, we have designed and built a confocal microscope PL system with high stability and temperature control, working in a range from 4 K to 300 K.

## Experimental Setup

The measurement system consists of the micro-PL head combined with the attoDRY700 cryostat and the excitation/detection optical system as illustrated in Figure 2. The micro-PL head is mounted inside the attoDRY700 chamber, as shown in the zoom out in Figure 2. The ML sample is loaded onto an XYZ stack of ANP positioners whose one end is fixed to the cold head of the cryostat. The objective is mounted on to the cold head providing the microscopic resolution and is used to focus the excitation laser as well as to collect the PL signal. For the TRPL measurements, picosecond pulses are generated from a frequency-doubled optical parametric oscillator (OPO) synchronously pumped by a mode-locked Ti:Sa laser. For the time-integrated PL measurements, continuous wave lasers with 633 nm and/or 532 nm wavelength are used. The excitation/detection

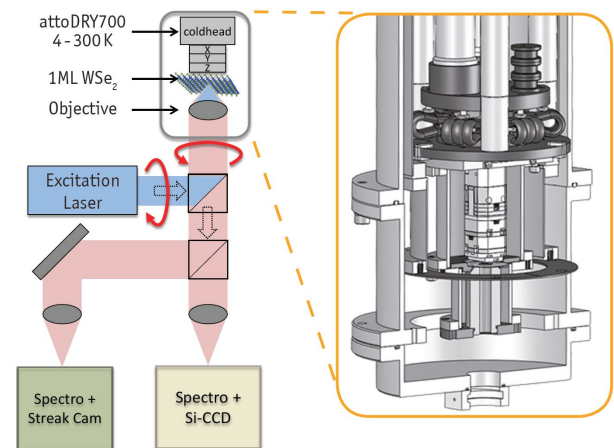


**Figure 2:** Schematics of the micro-PL setup.

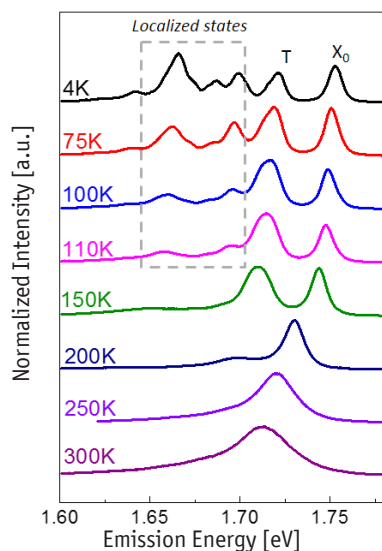


**Figure 3:** Temperature dependence of PL emission. Localized states can be seen up to a temperature of 110 K.

spot is around 1  $\mu\text{m}$  in diameter. The PL signal can be detected by a Hamamatsu streak camera with an overall time resolution of 4 ps for the TRPL or by a Si-CCD camera for the time-integrated PL. The co- (cross-) circular polarization component of the PL emission (with respect to the excitation laser) can be chosen by a quarter-wave plate placed in front of a linear polarizer. In this application note, right circularly polarized laser excitation ( $\sigma+$ ) will be used. The circular polarization is defined as  $P_C = (I_{\sigma+} - I_{\sigma-}) / (I_{\sigma+} + I_{\sigma-})$ , where  $I_{\sigma+}$  ( $I_{\sigma-}$ ) denotes the intensity of  $\sigma+$  ( $\sigma-$ ) components of the PL emission. The time evolution of  $P_C$  indicates the  $K$  valley dynamics of ML WSe<sub>2</sub>.

## Measurement Results

Integrated PL has been acquired from ML WSe<sub>2</sub> flake at different temperatures, as depicted in Figure 3. At low temperature ( $T = 4\text{ K}$ ), the PL contains emissions from neutral exciton  $X^0$ , trion and localized states. The narrow PL peak around 1.752 eV originate from the  $X^0$  and the trion energy is at 1.722 eV. This gives a larger trion binding energy of around 30 meV, which also demonstrates the strong Coulomb interaction inside 2D ML WSe<sub>2</sub>. PL emission from localized states, located at lower energy than the trion, vanishes when the temperature is raised to 110 K.

By fitting the TRPL results of the ML WSe<sub>2</sub> emission, we can extract the emission times of  $X^0$ , trion and localized states. Here we focus on the  $X^0$  and the trion emissions. The  $X^0$  emission decays so fast that it cannot be resolved by our setup. We infer a PL emission time shorter than 4 ps. Very different to the  $X^0$  the trion emission exhibits a first decay with a characteristic time of around 18 ps and a second decay with a characteristic time 30 ps.

Next we discuss the evolution of the circular polarization of the  $X^0$  and trion emissions, which is due to the initial valley population decay. Limited by the time resolution of our setup, we cannot extract the  $X^0$  valley depolarization time. As shown in Figure 4(a), the fast polarization decay happens already within the first 4 ps range. This is further confirmed in time-resolved Kerr rotation experiments with a femto-second laser [4]. The efficient  $X^0$  depolarization can be attributed to a strong Coulomb exchange coupling between the neutral excitons in  $K+$

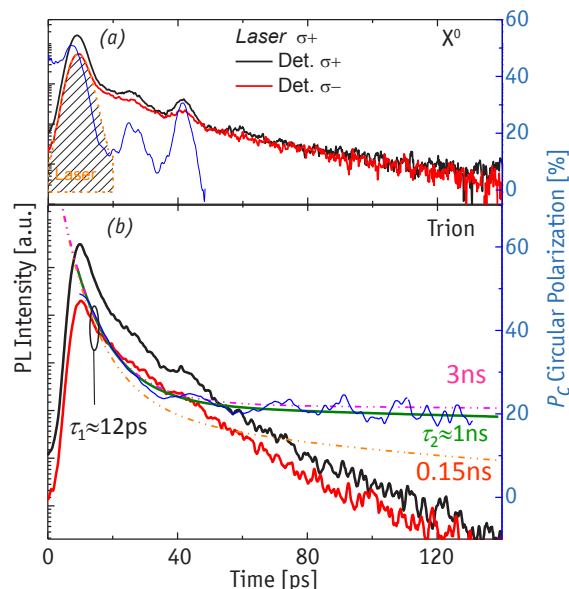


**Figure 4:** Time-resolved PL under  $\sigma+$  polarized laser excitation. Left axis: PL emission intensity. Right axis: circular polarization of PL emission. (a) Measured on  $X^0$ . (b) Measured on trion. Biexponential decay with  $\tau_1 = 12\text{ ps}$ ,  $\tau_2 = 1\text{ ns}$  (solid green line) is shown. Two other decay lines with  $\tau_2 = 0.15\text{ ns}$  (dotted orange line) and  $\tau_2 = 3\text{ ns}$  (dotted purple line) are plotted for comparison [5].

and  $K-$  valleys. The valley depolarization therefore does not dependent on single carrier spin flips. These are strongly suppressed by the conduction and valence band spin splittings in the meV and hundreds of meV range, respectively.

The valley polarization of the trion decays partially within 12 ps and then a stable plateau of 20% polarization is reached as depicted in Figure 3(b). The first, fast polarization decay has its origin possibly in the coexistence of the trion and the depolarized  $X^0$ . For the decay of the remaining, stable trion polarization a characteristic time as long as 1 ns can be inferred. In the trion case, the depolarization relies on the single particle spin flips and the scattering between the nonequivalent valleys, which is energetically too costly due to the large spin splittings. Stable valley polarization is clearly observed in the TRPL experiments on trions in monolayer WSe<sub>2</sub>.

## Summary

In this application note we show time-integrated, as well as time-resolved PL results for monolayer WSe<sub>2</sub> in a homemade micro-PL setup based on an attoDRY700 cryostat and ANP positioners. The time evolution of the circular polarization of the PL allows to probe the  $K$ -valley dynamics of the neutral and charged excitons (trions). Our results demonstrate the robustness of the optically generated valley polarization through the ns decay time of the trion polarization. This stable valley polarization will allow to further progress our understanding of the interaction between monolayer TMDCs and polarized light for applications and fundamental research.

## References

- [1] Wikipedia: [http://en.wikipedia.org/wiki/Transition\\_metal\\_dichalcogenide\\_monolayers](http://en.wikipedia.org/wiki/Transition_metal_dichalcogenide_monolayers)
- [2] M. M. Glazov *et al.*, Phys. Rev. B **89**, 201302 (2014).
- [3] G. Wang *et al.*, Phys. Rev. B **90**, 075413 (2014).
- [4] C. R. Zhu *et al.*, Phys. Rev. B **90**, 161302 (2014).
- [5] Figure reprinted with permission from G. Wang *et al.*, Phys. Rev. B **90**, 075413 (2014). Copyright 2014 by the American Physical Society.